Proceedings of the EPSRC/BBSRC International Workshop on
Biologically Inspired Robotics - The Legacy of W. Grey Walter,
14–16 August 2002, HP Labs Bristol, UK, pp. 196–203 (2002)

Behavior-Oriented Vision for Biomimetic Flight Control

Titus R. Neumann* **and Heinrich H. Bülthoff**
Max Planck Institute for Biological Cybernetics
Spemannstraße 38
72076 Tübingen, Germany
titus.neumann@tuebingen.mpg.de

Abstract

Most flying insects extract information about their spatial orientation and self-motion from visual cues such as global patterns of light intensity or optic flow. We present an insect-inspired neuronal filter model and show how optimal receptive fields for the detection of flight-relevant input patterns can be derived directly from the local receptor signals during typical flight behavior. Using a least squares principle, the receptive fields are optimally adapted to all behaviorally relevant, invariant properties of the agent and the environment. In closed-loop simulations in a highly realistic virtual environment we show that four independent, purely reactive mechanisms based on optimized receptive fields for attitude control, course stabilization, obstacle avoidance and altitude control, are sufficient for a fully autonomous and robust flight stabilization with all six degrees of freedom.

1 Introduction

The main idea of behavior-oriented vision is to extract only such information from the environment which is required to control a specific behavior. This allows to minimize the required amount of computation and internal representation. In particular, certain reactive behaviors can be immediately controlled by an appropriately selected visual input. As an example, phototropic reactions can be observed even in the most primitive animals, and were the first to be implemented in biologically inspired, autonomous robots (Walter, 1950). Braitenberg (1984) showed that the interaction of such simple, reactive mechanisms with the environment may lead to apparently complex behavior.

Since natural evolution optimizes the entire organism for specific behaviors in specific environments, analyzing biological examples may provide useful ideas and inspiration for artificial systems on various levels, including sensor morphology, processing steps, control mechanisms, and behavioral modules. Insect vision and behavior has been investigated for decades and many of the involved mechanisms are well understood. Flying insects are highly optimized for flight behavior in their natural environment. Thus in order to control an artificial flying system in a comparable environment, many aspects of insect vision and information processing can be imitated and do not need to be re-invented or developed from scratch.

Various reactive control mechanisms have been modeled in insect-inspired robots and computer simulations. Visual tracking was investigated in a simulation study by Cliff (1992). Mura and Franceschini (1994) simulated altitude control and vertical obstacle avoidance behavior, assuming pure forward translation in a vertical plane and fixed attitude angles. Weber, Venkatesh, and Srinivasan (1997) implemented horizontal centering behavior and speed control on a mobile robot. One-dimensional tracking and orientation towards a strong contrast was demonstrated by Huber, Franz, and Bülthoff (1999).

In previous studies we have shown that basic 3D flight stabilization can be achieved by a combination of four insect-inspired visual orientation strategies (Neumann & Bülthoff, 2001). These strategies include the dorsal light response for attitude control (Hengstenberg, Sandemann, & Hengstenberg, 1986), the optomotor response for course stabilization (Götz, 1968), as well as visual range finding from translatory image motion for obstacle avoidance and altitude control (Srinivasan, 1993; Srinivasan, Zhang, Chahl, Barth, & Venkatesh, 2000).

Here we demonstrate how the behavior-oriented extraction of visual information from the environment by wide-field integration units can be optimized in the sense of least squares, exploiting the covariance of input signals and behavior. In contrast to an earlier study on self-motion estimation (Franz, Neumann, Plagge, Mallot, & Zell, 1999), the optimal receptive fields are derived directly from the visual input and do not require an explicit model of the distance or contrast distributions in the environment. We present optimal receptive fields for each stabilization mechanism, as well as first closed-loop results showing that these mechanisms are capable of producing robust flight behavior with all six degrees of freedom in a highly realistic virtual environment.

*corresponding author

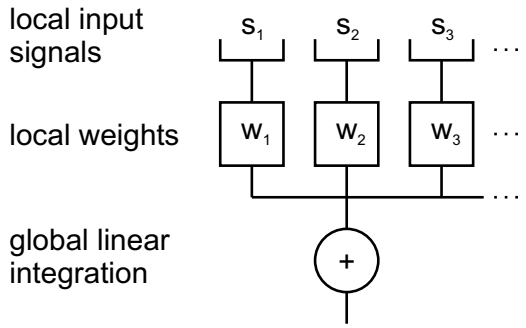

Figure 1: Linear wide field integration unit.

2 Extracting flight-relevant information from visual cues

2.1 Wide-field integration units

Insects use wide-field integration units to evaluate the local light intensity and local optic flow signals from preceding retinotopic processing steps. These units have complex receptive fields that are highly selective for behaviorally relevant input patterns. Their sensitivity distributions contain *a priori* information on invariant properties of both the behavior and the environment. Examples are the fly tangential neurons which are tuned to characteristic, self-motion-induced optic flow fields (Krapp & Hengstenberg, 1996).

A model for wide-field integration units is depicted in Fig. 1. A large population of locally weighted input signals is integrated to yield the receptive field response r as the scalar product

$$r = \sum_i w_i s_i = \mathbf{ws} \tag{1}$$

of the input signal vector $\mathbf{s}$ and the weight vector $\mathbf{w}$. To control the different components of flight behavior, various integration units evaluate the input signal distribution in parallel, each unit tuned to a specific pattern determined by the particular distribution of local weights.

Based on this general processing architecture inspired by the fly visual system, the exact weight distributions are determined using an optimization method. In the following, we show how optimal global receptive fields can be derived directly from the local receptor signals occurring during typical behavior. Using a least squares principle, the sensitivity distributions are optimally adapted to all behaviorally relevant, invariant properties of the agent and the environment, such as systematic errors in the motion detector signals, typical movements of the agent, and characteristic distributions of light intensity, color, contrast and distance in the environment.

2.2 Optimal receptive fields

Let $\mathbf{r} \in \Re^m$ be the vector of activation signals for a single motor unit, recorded at m measurements during typical behavior, and $\mathbf{S} \in \Re^{m\times(n+1)}$ the matrix containing the corresponding signals from n local receptors. Assuming a linear wide-field integration unit with weight vector $\mathbf{w} \in \Re^{n+1}$, the receptive field response is

$$\mathbf{r} = \mathbf{Sw}\,. \tag{2}$$

$\mathbf{S}$ cannot be inverted directly since $m > n+1$, so in order to obtain the weight vector $\mathbf{w}$, the Moore-Penrose inverse $\mathbf{S}^+$ has to be used instead and gives an optimal solution

$$\mathbf{w} = \mathbf{S}^+\mathbf{r} \tag{3}$$

in the sense of least squares, so we obtain the vector $\mathbf{w}$ with $\|\mathbf{Sw} - \mathbf{r}\| = \min$ (Press, Teukolsky, Vetterling, & Flannery, 1992).

The Moore-Penrose inverse can be efficiently calculated using a Singular Value Decomposition (SVD; Press et al., 1992). The SVD of the data matrix $\mathbf{S} \in \Re^{m\times(n+1)}$ yields three matrices $\mathbf{U} \in \Re^{m\times(n+1)}$, $\Sigma \in \Re^{(n+1)\times(n+1)}$ and $\mathbf{V} \in \Re^{(n+1)\times(n+1)}$ with

$$\mathbf{S} = \mathbf{U}\Sigma\mathbf{V}^{\mathrm{T}}\,. \tag{4}$$

The diagonal matrix Σ contains the singular values σ_i. The inverse

$$\tilde{\Sigma} = [\mathrm{diag}\,(\tilde{\sigma}_i)] \tag{5}$$

is determined by inverting the diagonal elements

$$\tilde{\sigma}_i = \begin{cases} 1/\sigma_i, & \sigma_i > \theta \\ 0, & else \end{cases}\,. \tag{6}$$

Singular values below a threshold θ are set to zero. Since $\mathbf{U}$ and $\mathbf{V}$ are orthogonal, they can be inverted by transposing, and we yield the Moore-Penrose inverse

$$\mathbf{S}^+ = \mathbf{V}\tilde{\Sigma}\mathbf{U}^{\mathrm{T}} \tag{7}$$

and the optimal weight vector

$$\mathbf{w} = \mathbf{V}\tilde{\Sigma}\mathbf{U}^{\mathrm{T}}\mathbf{r}\,. \tag{8}$$

However, the high dimensionality of the data matrix $\mathbf{S}$ impedes the numerical tractability of the SVD. As an example, for altitude control the output signals of 1920 elementary motion detectors are recorded at 1000 randomly selected locations in the virtual environment, each measurement for 10 time steps with a randomly chosen altitude, resulting in a very large data matrix $\mathbf{S} \in \Re^{10000\times1921}$.

The dimensionality can be reduced by recording $\mathbf{S}^{\mathrm{T}}\mathbf{r} \in \Re^{n+1}$ instead of $\mathbf{r} \in \Re^m$ and $\mathbf{S}^{\mathrm{T}}\mathbf{S} \in \Re^{(n+1)\times(n+1)}$ instead of $\mathbf{S} \in \Re^{m\times(n+1)}$. Eq. (2) then becomes

$$\mathbf{S}^{\mathrm{T}}\mathbf{r} = \mathbf{S}^{\mathrm{T}}\mathbf{Sw}\,, \tag{9}$$

and with the Moore-Penrose inverse $\left(\mathbf{S}^{\mathrm{T}}\mathbf{S}\right)^+$ we obtain

$$\left(\mathbf{S}^{\mathrm{T}}\mathbf{S}\right)^+\mathbf{S}^{\mathrm{T}}\mathbf{r} = \left(\mathbf{S}^{\mathrm{T}}\mathbf{S}\right)^+\mathbf{S}^{\mathrm{T}}\mathbf{Sw}\,, \tag{10}$$

Figure 2: Virtual environment used in the simulation experiments.

hence the weight vector is

$$\mathbf{w} = \left(\mathbf{S}^{\mathrm{T}}\mathbf{S}\right)^{+}\mathbf{S}^{\mathrm{T}}\mathbf{r}\,. \tag{11}$$

Again we use the SVD

$$\mathbf{S}^{\mathrm{T}}\mathbf{S} = \mathbf{U}\Sigma\mathbf{V}^{\mathrm{T}} \tag{12}$$

to yield the Moore-Penrose inverse

$$\left(\mathbf{S}^{\mathrm{T}}\mathbf{S}\right)^{+} = \mathbf{V}\tilde{\Sigma}\mathbf{U}^{\mathrm{T}} \tag{13}$$

and finally the optimal weight vector

$$\mathbf{w} = \mathbf{V}\tilde{\Sigma}\mathbf{U}^{\mathrm{T}}\mathbf{S}^{\mathrm{T}}\mathbf{r}\,. \tag{14}$$

In principle, this method allows to record time series of arbitrary length since $\mathbf{S}^{\mathrm{T}}\mathbf{r}$ and $\mathbf{S}^{\mathrm{T}}\mathbf{S}$ remain at a constant size. In practice, however, the numerical stability of the SVD depends on the 'condition number' (Press et al., 1992), the ratio of the largest and the smallest singular value occurring in Σ. The condition number rapidly increases with an increasing number of measurements m, which might lead to errors for $m \gg n$.

3 Simulation setup and implementation

All experiments were implemented as computer simulations on a standard PC equipped with 3D OpenGL graphics acceleration for polygon-based, textured rendering of highly detailed scenes. The generated, highly realistic visual stimuli were used for both the receptive field optimization and the subsequent closed-loop evaluation of the entire processing system.

3.1 Virtual environment

Fig. 2 shows an example view of the virtual environment used in the simulation experiments. The simulated environment is composed of a highly realistic, three-dimensional landscape with an uneven, hilly terrain and randomly placed trees. All visible objects such as terrain, obstacles and sky exhibit a detailed, high-resolution and nonperiodic surface texture with local variations in luminance, color, contrast and spatial frequency.

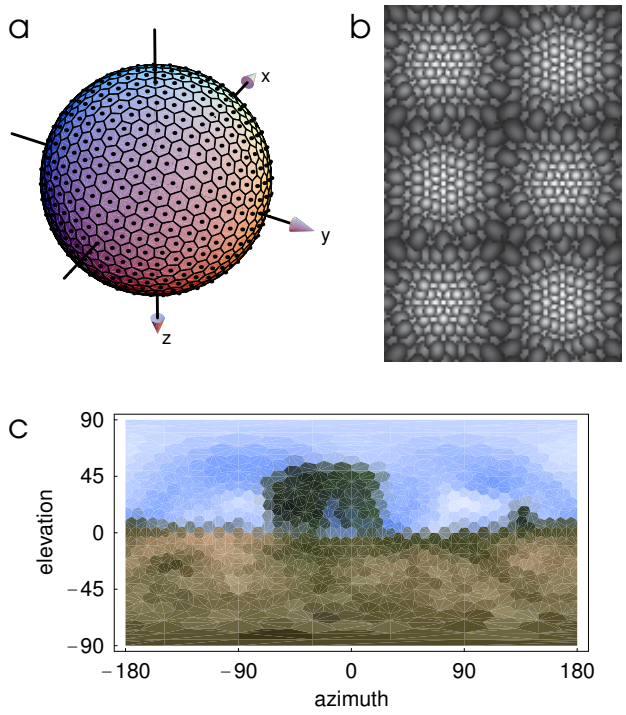

Figure 3: Insect inspired omnidirectional eye model. *a*. Receptor distribution. *b*. Spherical image acquisition from six perspective views. *c*. Virtual landscape seen through the spherical eye.

3.2 Eye model

Visual stimuli are retrieved from the virtual environment by an insect-inspired, omnidirectional eye model. It incorporates typical properties of insect compound eyes, such as an omnidirectional distribution of discrete light receptors in a spherical field of view, low image resolution, and overlapping local receptive fields of the individual receptor units.

Fig. 3*a* shows a quasi-homogeneous distribution of 642 local viewing directions on the sphere, arranged on a hexagonal lattice. Using this eye model, low-resolution, spherical images are generated by downsampling from multiple perspective views of the environment, taken at the current eye position. All local receptor units have appropriately distorted, overlapping Gaussian-shaped sensitivity distributions (Fig. 3*b*) in order to prevent spatial aliasing. Fig. 3*c* shows the virtual landscape as seen through the spherical eye. The image covers the entire sphere surrounding the current eye position, ranging from -180° to 180° azimuth and from -90° to 90° elevation. The increasing distortions toward the poles are due to the Mercator projection used for visualization and do not occur in the original spherical image.

3.3 Local motion detection

After the distribution of light intensities has been determined according to the eye model, an additional omnidirectional image containing the spherical distribution of local image mo-

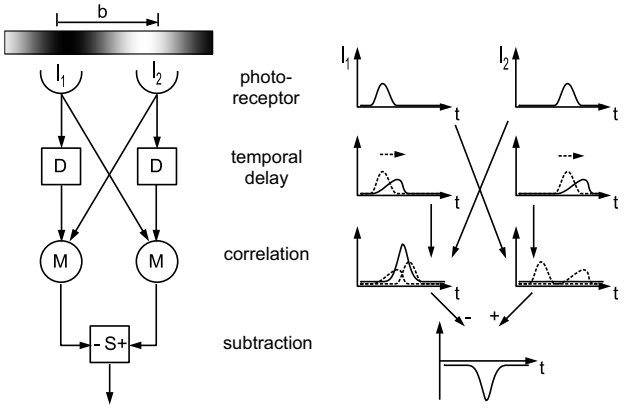

Figure 4: Elementary correlation-type motion detector after Hassenstein and Reichardt (1956).

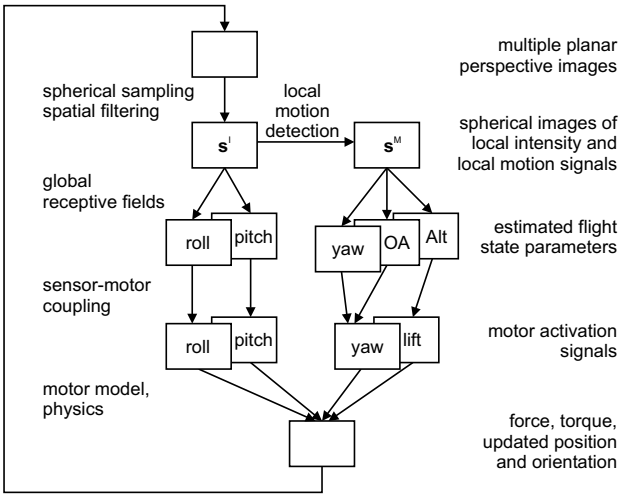

Figure 5: Visual processing and flight control loop. Arrows represent processing stages, rectangles the output data generated by each stage.

tion is calculated in a subsequent processing step.

As in previous studies (Neumann & Bülthoff, 2001), insect-inspired, elementary motion detectors (EMDs) of the correlation-type after Hassenstein and Reichardt (1956) are placed between adjacent photoreceptors. As illustrated in Fig. 4, two neighboring photoreceptors detect the image intensities I_1 and I_2. In each of two mirror-symmetric semidetectors one of these input signals is delayed by a temporal low pass filter and subsequently correlated with the other, undelayed signal. The detector response is maximal when the image displacement during the temporal delay equals the angular distance between the two photoreceptors. The sign of the difference between both semidetector responses indicates the direction of motion.

3.4 Flight control loop

The control architecture of the flying agent includes multiple processing stages and is depicted in Fig. 5. The low resolution spherical images of local light intensities and local optic flow serve as input signals for the wide-field integration units in the subsequent processing step. These units are tuned to specific patterns in the input signal distribution which are immediately relevant for the control of specific behaviors. In particular, they are optimized to estimate roll and pitch attitude angles directly from the omnidirectional intensity distribution, as well as yaw rotations and the relative nearness of objects in the frontolateral and ventral visual field from the local optic flow signals. The exact sensitivity distributions resulting from the optimization procedure described above are presented in the following section.

The output values of the wide-field integration units are immediately used to modulate motor activations that compensate for deviations from the desired flight state. Inertial properties of the flying agent are ignored in this simulation. Small flying insects experience strong viscous air resistance and reach a steady state velocity after a short initial acceleration phase (Nachtigall, 1968). Thus to a first approximation, the velocity of the agent is set proportional to the generated lift and thrust forces. The control loop is closed by updating the position and orientation of the agent in the environment.

4 Results

The control architecture of the flying agent is composed of four independent behavioral modules, including attitude control, course stabilization, obstacle avoidance and altitude control. The crucial processing element for each of these subbehaviors is a highly specialized global integration unit that extracts the required information from the spherical distribution of local input signals. In this section we present the exact sensitivity distributions of these units resulting from the described optimization method. Furthermore, examples for closed-loop flight behavior based on these mechanisms are shown.

4.1 Optimal receptive fields

For each target behavior, 10000 complete, spherical images of local intensity or local motion signals were recorded at randomly chosen locations in the virtual environment. The according motor activations were varied within the limits that typically occur during free flight situations, and recorded together with the simultaneously perceived visual stimuli. From these data, optimal linear receptive fields were determined using the optimization procedure described in Section 2. The resulting sensitivity distributions are presented in the following.

Attitude angles

In our simulation the dynamic range of luminance is smaller than in the real world. To compensate, vertical color gra-

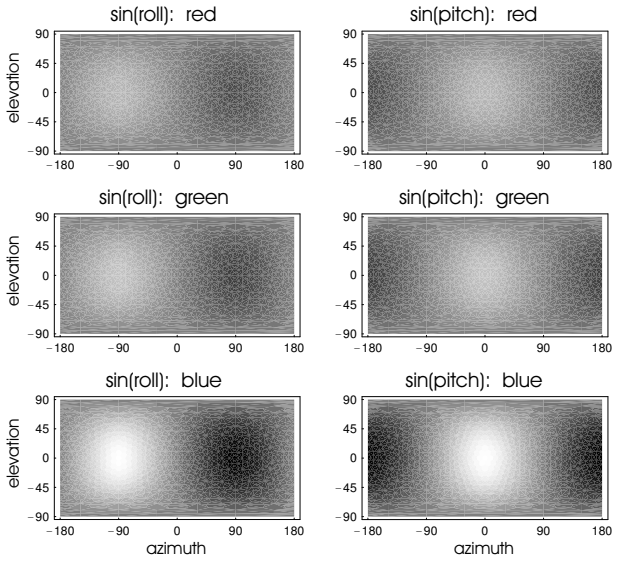

Figure 6: Optimal spherical receptive fields for attitude estimation. Dark regions indicate negative, bright regions positive weights.

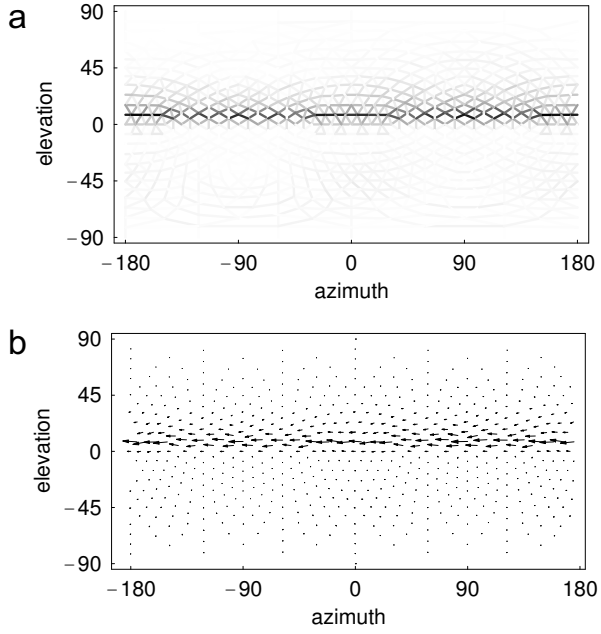

Figure 7: Optimal receptive field for yaw rotations. *a*. Spherical weight distribution for local EMD signals. Darker lines indicate higher values. *b*. Corresponding optic flow field.

dients are exploited instead of a luminance gradient. Fig. 6 shows spherical receptive fields for attitude estimation from the momentary color distribution around the agent. The local weights for the red, green and blue receptors are shown in separate gray value images. Dark regions indicate negative and bright regions positive weights. The highest sensitivity is assigned to the blue component since the sky color is almost position invariant and therefore indicates the world vertical more reliably than the variable and position dependent ground colors.

The receptive fields are optimized to estimate the sines of the roll (left column) and pitch (right column) angles. Thus, the output values indicate the direction of deviation from neutral attitude and can be immediately used as negative feedback signals for attitude control. The shown spatial sensitivity distributions resemble those of insect *ocelli*, which are involved in the dorsal light response of some insects (Schuppe & Hengstenberg, 1993).

Yaw velocity

An optimal receptive field for the detection of yaw rotations in the presence of simultaneous translatory forward motion is presented in Fig. 7*a*, showing the spherical weight distribution for the local EMD signals. The orientation of each line segment depicts the local EMD direction, the gray level indicates the scaled absolute value of the corresponding weight, darker lines representing higher values. Fig. 7*b* shows the corresponding optic flow field. The orientation of each arrow shows the local preferred direction, the length denotes the local relative sensitivity.

The receptive field is tuned to rotations about the vertical axis during forward flight. The local motion sensitivities are highest in the image region around the horizon, where the optic flow is largely independent of distance variations and translatory self-motion. The ventral region is exposed to strong translatory flow due to the smaller distance to the ground. In the dorsal region the insufficient contrast of the sky texture prevents a reliable motion detection. Thus, both regions do not correlate with yaw rotation and receive smaller weights. The output signal of this receptive field can be directly transmitted to the yaw motor to establish course stabilization behavior resembling the optomotor response in insects.

Relative nearness to obstacles

Optic flow fields induced by translatory self-motion contain information about the spatial layout of the environment as they depend not only on the velocity of the observer, but also on the distance of the observed objects. The depicted receptive field is tuned to detect differences of translatory optic flow in the left and right frontolateral regions of the visual field. The sign of the output signal indicates whether the relative object nearness is larger on the left or on the right side of the agent. Thus, it can be used to avoid potential obstacles by turning toward the direction of minimal image motion. Fig. 8 shows an optimal receptive field for frontolateral relative nearness difference.

Relative nearness to the ground

The receptive field shown in Fig. 9 is another example for visual range finding from translatory optic flow. It is specialized

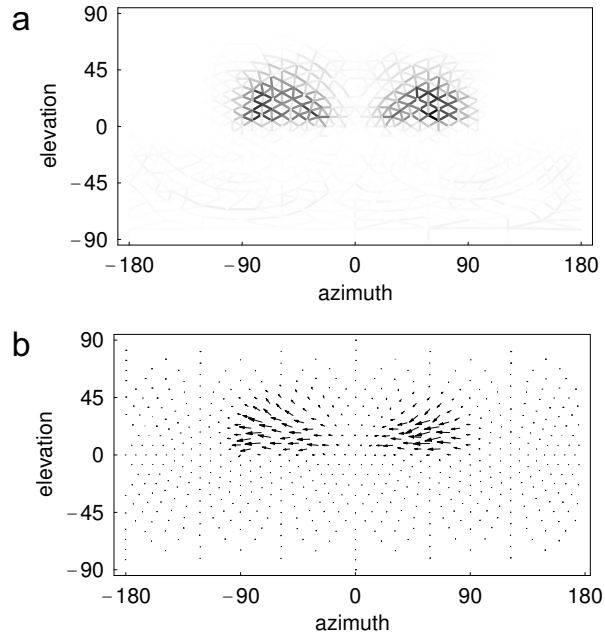

Figure 8: Optimal receptive field for frontolateral relative nearness difference. Details as in Fig. 7.

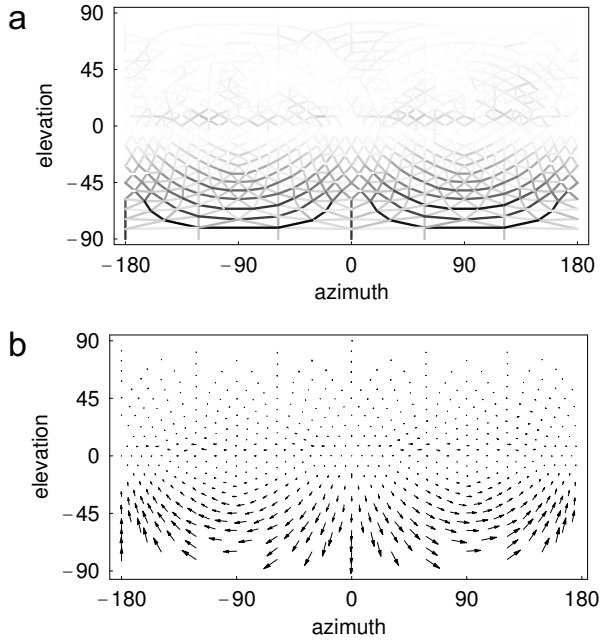

Figure 9: Optimal receptive field for relative ground nearness. Details as in Fig. 7.

on estimating the relative nearness of the agent to the ground plane. Naturally, this information is essential for altitude control and can be readily used to modulate the lift force. The highest correlations of EMD signals with the relative ground nearness occur in the ventral region of the visual field since the ground plane provides a high contrast texture and is close to the agent. Therefore, the largest weights are assigned to the ventral region.

4.2 Closed-loop flight behavior

All four behavioral modules were combined in a flying autonomous agent and tested in closed-loop experiments. The resulting trajectories (Fig. 10) show that the agent is capable of autonomous flight behavior with all six degrees of freedom in a highly realistic virtual environment. Full flight behavior requires that all mechanisms are active simultaneously. Contributions of single modules can be observed depending on the specific situation of the agent in the environment.

Attitude control. As a prerequisite for all other mechanisms, the dorsal light response ensures that the agent is always aligned with the terrain surface.

Course stabilization. In the absence of potential obstacles, yaw rotations are suppressed by the optomotor response. Therefore the agent moves along a straight path (Fig. 10*a*).

Obstacle avoidance. Strong frontolateral image motion during forward translation of the agent indicates a potential obstacle. The agent avoids a collision by turning toward the direction of smaller optic flow indicating a larger relative object distance (Fig. 10*b*).

Altitude control and terrain following. The optic flow in the ventral region of the visual field is used as an indicator for relative ground nearness, i.e. the reciprocal value of relative altitude. The agent follows the terrain elevation by increasing the lift force for strong ventral optic flow, reaching an "equilibrium altitude" when the lift force equals gravity (Fig. 10*c*). Slight oscillations in altitude can be observed when flying over regions with strong changes in texture luminance or contrast. In all situations, collisions with the ground or with obstacles are robustly avoided.

5 Discussion

We present a biologically motivated visual flight control system composed of four reactive orientation strategies including attitude control, course stabilization, altitude control and obstacle avoidance. Using a behavior-oriented approach, the entire vision system is designed to acquire and process only behaviorally relevant information in a highly selective manner. Since flying insects are optimized for flight behavior by natural evolution, they serve as exemplary systems for both the orientation strategies as well as the information acquisition and processing stages of the artificial vision system.

The orientation mechanisms are based on the evaluation of light intensity and optic flow patterns in a spherical field of view by highly specialized wide-field integration units inspired by fly tangential neurons. The covariance of local receptor signals and specific behaviors is used to optimize the sensitivity distributions of the global receptive fields to selectively extract flight-relevant information from the visual input. Explicit models of the distance or contrast distribution in the environment are not required since the weight distribu-

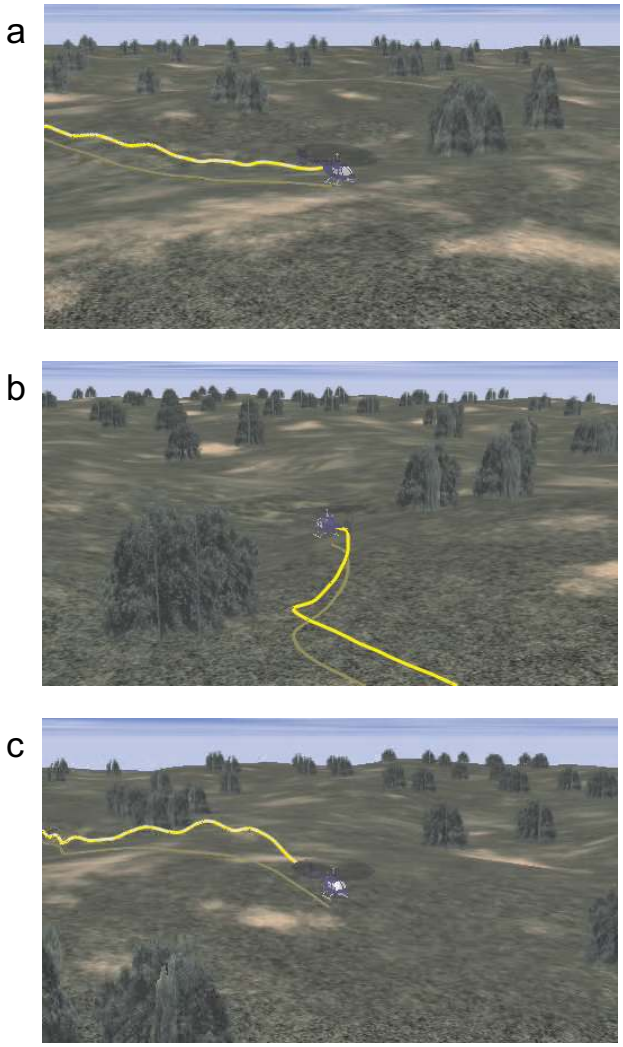

Figure 10: Closed-loop autonomous flight control with all six degrees of freedom. The trajectories are shown as bright lines, together with their projections on the terrain surface. The position and orientation of the flying agent is indicated by a small helicopter. *a*. Course stabilization. *b*. Obstacle avoidance. *c*. Altitude control and terrain following.

tions are derived directly from the input signals.

Our results encompass the exact sensitivity distributions of all involved global receptive fields. Furthermore, we present trajectories from closed-loop flight simulations showing that four independent, purely reactive visual orientation strategies are sufficient for robust 3D flight behavior in a highly realistic virtual environment. A detailed, quantitative analysis of the receptive field responses and the resulting flight behavior will be presented elsewhere (Neumann, in preparation).

5.1 Applications

All four mechanisms for visual flight stabilization presented above are purely reactive and do not require internal representations of the environment or trajectory planning. They are based on a massive parallel, feed-forward flow of information with few sequential processing steps, leading to robust behavior and short reaction times suitable for real-time control of autonomous robots. The connection and weighting schemes are highly optimized for specific tasks and do not change during computation, facilitating possible hardware implementations such as analog VLSI (Very Large Scale Integration). Simple, robust control algorithms are crucial for autonomous vehicle guidance and robotics, especially in applications with strong constraints in size, weight and energy consumption, such as aerospace and miniature robotics.

In analogy to the simulation experiments described here, the basic processing architecture of these robots can be based on the insect visual system, whereas the exact weight distributions are derived directly from the visual input during typical behavior in a typical environment. It is worth noting that the input images containing pre-processed local information such as luminance, color or local motion, may differ in size, shape or resolution. The optimization method ensures that the maximum amount of behaviorally relevant information is extracted even from arbitrary receptor arrangements.

5.2 Aerial Robotics

Real-world flying robots are subject to constraints in the available hardware platforms such as model planes, helicopters, or blimps. Most of these platforms are built at larger physical scales than flying insects. Therefore they may experience fundamentally different physical effects when interacting with the environment. In particular, the relative effect of viscous air resistance is strongly reduced in large scale robots compared to small flies. This has consequences for the applied orientation strategies and control algorithms:

- Large flying robots require a simultaneous visual control of both forward velocity as well as object and ground distance. In contrast, the forward velocity of small flying insects is to a first approximation proportional to the applied force.

- Inertial effects need to be actively compensated in large robots, whereas in small flies unintended self-motions relative to the surrounding air are passively inhibited by air resistance. In turn, robots are more robust against external influences like wind or turbulences, which require active compensation in insects.

- Many flying insects are physically more robust and tolerant against collisions than robots, and are therefore able to survive failures of the obstacle avoidance system. For most flying robots collisions are fatal due to the large mass and forces during impact. In addition, even a slight contact of the propulsion system with an obstacle may lead to severe damage or destruction of the flight platform. Thus, large-scale flying robots require an extremely

reliable mechanism for collision avoidance, whereas insects are inherently more tolerant against failures of the visual system.

Other issues such as onboard vibration require additional solutions, e.g., an appropriate adaptation of the spatiotemporal sampling and low pass filtering of the visual input signals to the properties of the particular robot and environment. The vision system proposed here is expected to be robust against onboard vibrations with small amplitude since it has a very coarse spatial resolution.

In conclusion, the described insect-inspired reactive control mechanisms are expected to perform best for applications such as micromechanic implementations or small underwater robots, which are subject to similar physical effects and constraints as real flies. Larger robots may require different control algorithms due to different motion dynamics and propulsion systems. Thus, miniature implementations or computer simulations may be more suitable models for flight control in insects than large flying robots. For all of these applications the proposed behavior-oriented vision system provides a simple but highly effective method to extract flight-relevant information from the environment.

Acknowledgments. We thank Matthias Franz and Roland Hengstenberg for helpful discussions, Kathrin Schrick for critical reading, and the anonymous reviewers for valuable comments.

References

Braitenberg, V. (1984). *Vehicles: Experiments in Synthetic Psychology*. MIT Press, Cambridge, MA, USA.

Cliff, D. (1992). Neural networks for visual tracking in an artificial fly. In Varela, F., & Bourgine, P. (Eds.), *Towards a Practice for Autonomous Systems: Proceedings of the First European Conference on Artificial Life (ECAL'91)*, pp. 78–87 Cambridge, MA. MIT Press Bradford Books.

Franz, M. O., Neumann, T. R., Plagge, M., Mallot, H. A., & Zell, A. (1999). Can fly tangential neurons be used to estimate self-motion?. In Willshaw, D., & Murray, A. (Eds.), *Proceedings of the 9th International Conference on Artificial Neural Networks (ICANN'99)*, Vol. CP 470, pp. 994–999. IEE, London.

Götz, K. G. (1968). Flight control in *Drosophila* by visual perception of motion. *Kybernetik*, *4*(6), 199–208.

Hassenstein, B., & Reichardt, W. (1956). Systemtheoretische Analyse der Zeit-, Reihenfolgen- und Vorzeichenauswertung bei der Bewegungsperzeption des Rüsselkäfers *Chlorophanus*. *Zeitschrift für Naturforschung B*, *11*(9/10), 513–524.

Hengstenberg, R., Sandemann, D. C., & Hengstenberg, B. (1986). Compensatory head roll in the blowfly *Calliphora* during flight. *Proceedings of the Royal Society of London B*, *227*(1249), 455–482.

Huber, S. A., Franz, M. O., & Bülthoff, H. H. (1999). On robots and flies: Modeling the visual orientation behavior of flies. *Robotics and Autonomous Systems*, *29*(4), 227–242.

Krapp, H. G., & Hengstenberg, R. (1996). Estimation of self-motion by optic flow processing in single visual interneurons. *Nature*, *384*, 463–466.

Mura, F., & Franceschini, N. (1994). Visual control of altitude and speed in a flying agent. In Cliff, D., Husbands, P., Meyer, J. A., & Wilson, S. W. (Eds.), *From Animals to Animats 3: Proceedings of the Third International Conference on Simulation of Adaptive Behavior (SAB'94)*, pp. 91–99 Cambridge, MA. MIT Press Bradford Books.

Nachtigall, W. (1968). *Insects in Flight*. McGraw-Hill, New York.

Neumann, T. R., & Bülthoff, H. H. (2001). Insect inspired visual control of translatory flight. In Kelemen, J., & Sosik, P. (Eds.), *Advances in Artificial Life, Proceedings of ECAL 2001*, Vol. 2159 of *LNCS/LNAI*, pp. 627–636. Springer-Verlag, Berlin.

Press, W. H., Teukolsky, S. A., Vetterling, W. T., & Flannery, B. P. (1992). *Numerical recipes in C*. Cambridge University Press, Cambridge, U.K.

Schuppe, H., & Hengstenberg, R. (1993). Optical properties of the ocelli of *Calliphora erythrocephala* and their role in the dorsal light response. *Journal of Comparative Physiology A*, *173*(2), 143–149.

Srinivasan, M. V. (1993). How insects infer range from visual motion. In Miles, F. A., & Wallman, J. (Eds.), *Visual Motion and its Role in the Stabilization of Gaze*, pp. 139–156. Elsevier, Amsterdam.

Srinivasan, M. V., Zhang, S. W., Chahl, J. S., Barth, E., & Venkatesh, S. (2000). How honeybees make grazing landings on flat surfaces. *Biological Cybernetics*, *83*(3), 171–183.

Walter, W. G. (1950). An imitation of life. *Scientific American*, *May 1950*, 42–45.

Weber, K., Venkatesh, S., & Srinivasan, M. V. (1997). Insect inspired behaviours for the autonomous control of mobile robots. In Srinivasan, M. V., & Venkatesh, S. (Eds.), *From Living Eyes to Seeing Machines*, pp. 226–248. Oxford University Press, Oxford, New York.